International Journal of Mass Spectrometry 299 (2011) 13–19

Contents lists available at ScienceDirect

International Journal of Mass Spectrometry

journal homepage: www.elsevier.com/locate/ijms

Recognizing *ortho*-, *meta*- or *para*-positional isomers of S-methyl methoxylphenylmethylenehydrazine dithiocarboxylates by ESI-MS^2: The positional effect of the methoxyl substituent

Kezhi Jiang[a,b], Gaofeng Bian[b], Yuanjiang Pan[a,*], Guoqiao Lai[b]

[a] Department of Chemistry, Zhejiang University, 38#, Zheda Road,Hangzhou 310027, China
[b] Key Laboratory of Organosilicon Chemistry and Material Technology, Hangzhou Normal University, 222# Wenyi Road, Hangzhou 310012, China

ARTICLE INFO

Article history:
Received 8 May 2010
Received in revised form 1 September 2010
Accepted 3 September 2010
Available online 15 September 2010

Keywords:
Isomer differentiation
ESI-MS/MS
The positional effect of methoxyl substituent
DFT calculation

ABSTRACT

The dissociation chemistry of the *ortho*-, *meta*- or *para*-isomers of protonated S-methyl methoxyl- (or chloro-) benzenylmethylenehydrazine dithiocarboxylate, RPhCH=N–NHC(=S)–SCH_3 (R = MeO– or Cl–), has been investigated by collision induced dissociation experiments and DFT theoretical calculations. The three methoxyl-substituted isomers were easily differentiated according to the different abundance of the characteristic ion at *m/z* 136, resulting from the varying reactivity of the (NSC)SCH_3 elimination. This fragmentation is triggered by the positive charge upon protonation on the imine N2. Relative to the *meta* isomer, the positive charge on N2 in the *para* isomer is dispersed due to the electron donating resonance of the methoxyl group, which leads to higher energy barrier in the dissociation reaction and the less abundant product ion (*m/z* 136) in the MS/MS. (NSC)SCH_3 elimination of the *ortho*- isomer is further suppressed due to both the resonance effect and the "ortho effect" (an intramolecular hydrogen bond), with much higher energy barrier and extremely lower abundance of the fragment ion (*m/z* 136, 0.4%). The chloro substituted isomers, however, are short of the above positional effects due to the weak electronic effect of the substituent, and share the similar tandem mass spectrum.

1. Introduction

The positional pattern of substituents, such as *ortho*/*meta*/*para*, frequently exerts a significant effect on the chemical behavior [1–6] and even the biological action of a compound based on its efficacy and/or toxicity [7–10]. The unambiguous structural identification of isomeric compounds from either chemical synthesis or natural source is very crucial in the field of chemistry, pharmaceutics, and toxicology. Isomer separation and differentiation also becomes a very important and attractive analytical issue [11–22]. To develop MS-based-only methods for recognizing isomers is fascinating and interesting, which will benefit from the superiorities of mass spectrometry, such as rapidity, sensitivity and selectivity [23–27]. Although isomers share exactly the same mass, they can sometimes be distinguished solely by MS methods, due to the different fragmentation behaviors of their structurally diagnostic ion under the same conditions. Many *ortho* isomers of aromatic compounds can be relatively easily recognized in the EI spectrum, due to the so-called "*ortho* effect" [13–15]. A methodology for general recognition of constitutional isomers based on structurally diagnostic fragment ions has been proposed [28–30].

Most of above examples have all been preformed on EI-MS or CI-MS. Distinction of positional isomers is needed to develop based on electrospray ionization mass spectrometry (ESI-MS), since it has become an indispensable tool for the analysis of a large variety of compounds, especially in drug discovery and drug metabolism [31–33]. And it is much attractive to further investigate the mechanism of the positional effect on the reactivity of the structurally diagnostic ion, which will be helpful to find a rule to differentiate the analogical isomers.

S-methyl substituted phenylmethylenehydrazine dithiocarboxylate, a Shiff base resulted from substituted phenyl aldehyde, shows particular biological activities, such as antibacterial and anticancer nature, and becomes an important functional group of many drug molecules [34,35]. Decomposition of its neutral and protonated analogs has been investigated in detail in our earlier work [36,37]. We herein report differentiation of the three positional isomers of its methoxyl-substituted derivatives solely by ESI-MS/MS techniques, in which dissociation of the protonated molecule generates a significant variation in product ion ratios in the tandem mass spectrum. The mechanisms of the positional effect on the reactivity of the molecular ion have also been investigated in detail by DFT theoretical calculation.

* Corresponding author.
E-mail addresses: panyuanjiang@zju.edu.cn (Y. Pan), gqlai@hznu.edu.cn (G. Lai).

1387-3806/$ – see front matter © 2010 Elsevier B.V. All rights reserved.
doi:10.1016/j.ijms.2010.09.004

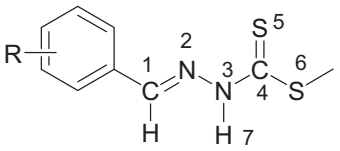

R = *o*-MeO *o*-M_1, R = *o*-Cl *o*-M_2,
R = *m*-MeO *m*-M_1, R = *m*-Cl *m*-M_2,
R = *p*-MeO *p*-M_1, R = *p*-Cl *p*-M_2.

Scheme 1. Structure of S-methyl methoxyl- (or chloro-) substituted benzenylmethylenehydrazine dithiocarboxylates.

2. Experimental

2.1. Materials

The positional isomers of interest, S-methyl substituted benzenylmethylenehydrazine dithiocarboxylates, RPhCH=N–NHC(=S)SCH_3 (R = MeO–, Cl–) (Scheme 1), were synthesized in our laboratory, with the methoxyl or chloro substituent at different position on the phenyl group. The samples were purified by wash with *i*-PrOH and recrystallization from CH_2Cl_2 and identified by MS and NMR [34,38].

2.2. Mass spectrometry

Analysis of the samples was performed on an LCQ advantage mass spectrometer (ThermoFisher Company, USA), equipped with an ESI ion source in the positive ionization mode, with data acquisition using the Xcalibur software (Version 1.4). Typical parameters were used for operation of the ESI-MS as follows:

The compounds were dissolved in a mixed reagent of methanol and water (V:V = 1:1) at a concentration of about 10 ppm. The diluted solutions were introduced into the source chamber via a length of 50 μm i.d. × 190 o.d. fused-silica tubing at a flow rate of 5 μL min^{-1}. A potential of −4.5 kV and a sheath gas of nitrogen at a pressure of 25 bar were employed. The heated capillary was maintained at 250 °C. The collision induced dissociation mass spectrometry (CID-MS) of the protonated molecules were obtained with helium as the collision gas after isolation of the precursor ions, and the relative collision energy was set at 20% [39]. All data points collected were the average of 50 scans.

2.3. Theoretical calculations

The theoretical calculations were performed with the Gaussian 03 program [40]. The equilibrium geometries of reactants, transition states, intermediates and products were optimized, by using the density functional theory (DFT) method at the B3LYP/6-31+G(2d,p) level, with the calculated force constants. No symmetry constraint was imposed in the optimization. All reactants, intermediates and products were identified as true minima by the absence of imaginary frequencies. Transition state, on the other hand, was identified by the presence of one single imaginary vibration frequency and the normal vibrational mode. Transition states were further confirmed by the intrinsic reaction coordinates (IRC) calculations. Vibrational frequencies and zero-point energies (ZPE) for all the key species were calculated at the same level of theory. The DFT optimized structures were shown by Gauss View (Version 3.09) software to give higher quality images of these structures.

Hard data on geometries of all structures considered are available as Supplementary material. The corresponding Gibbs free energies (at 298 K) are presented in Tables 2 and 3.

3. Experimental results and discussion

Fig. 1 shows the tandem mass spectra of the three methoxyl-substituted isomers (*o*-, *m*- and *p*-M_1 in Scheme 1) under the same conditions as described the experimental section. All the protonated molecule (*m/z* 241) undergoes two main fragmentations, similar to that of the protonated S-methyl benzenylmethylenehydrazine dithiocarboxylates [37]. The most abundant fragment ion *m/z* 193 is generated via elimination of CH_3SH of the precursor ion, and the other product ion *m/z* 136 formed via elimination

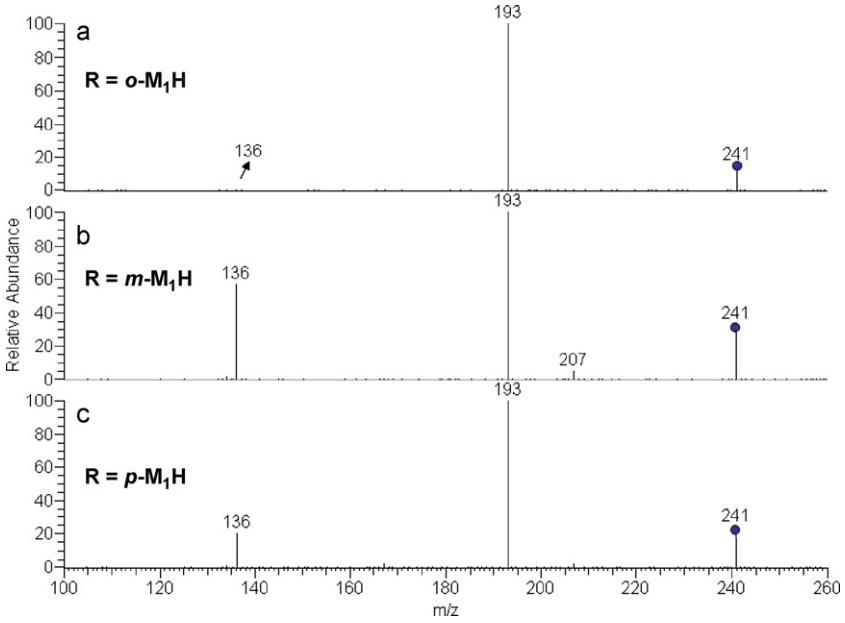

Fig. 1. The MS/MS of the protonated molecule $[M+H]^+$ for the three positional isomers (a: *ortho*-, b: *meta*-, and c: *para*-) of S-methyl methoxylbenzenylmethydenehydrazine dithiocarboxylate at the relative CID energy of 20%.

Table 1
Main product ions observed in the ESI-MS/MS of the protonated title compounds, at the relative CID energy of 20%.

Compounds	Substituent	$[M+H]^+$	Product ions *m/z* (%)		
	(R)	*m/z* (%)	Losing H_2S	Losing CH_3SH	Losing (NSC)SCH_3
***o*-M$_1$**	*o*-OCH_3	241 (25.3%)	207 (0.1%)	193 (100%)	136 (0.4%)
***m*-M$_1$**	*m*-OCH_3	241 (34.3%)	207 (3.8%)	193 (100%)	136 (57.7%)
***p*-M$_1$**	*p*-OCH_3	241 (24.7%)	207 (1.4%)	193 (100%)	136 (22.0%)
***o*-M$_2$**	*o*-Cl	245 (53.8%)	211 (4.0%)	197 (100%)	140 (33.2%)
***m*-M$_2$**	*m*-Cl	245 (53.0%)	211 (9.6%)	197 (100%)	140 (45.6%)
***p*-M$_2$**	*p*-Cl	245 (58.6%)	211 (4.9%)	197 (100%)	140 (49.5%)

of (NSC)SCH_3. The detailed tandem MS data are summarized in Table 1.

Interestingly, the relative abundance of the product ions is significantly affected by the positional pattern of the methoxyl substituent. As shown in Fig. 1, the fragment ion (*m/z* 136) resulting from dissociation of the *meta*-isomer are distinctly more abundant than that from the *para*- one (57.7% in ***m*-M$_1$** versus 22.0% in ***p*-M$_1$**), due to the different substituent site of the methoxyl group with strong electronic effect. The relevant fragment ion (*m/z* 136) from the *ortho*-isomer, however, is extremely low in abundance (0.4%) due to the "*ortho* effect" [13–15]. In addition, the precursor ion (*m/z* 241) of **[*m*-M$_1$+H]$^+$** is relatively more abundant than that of the other isomers. A minor product ion (*m/z* 207, 3.8%), resulting from elimination of H_2S [37], is also more easily observed in the MS/MS of **[*m*-M$_1$+H]$^+$**. As a result, the three methoxyl-substituted isomers can be differentiated solely by tandem MS.

To further investigate their different fragmentation behaviors, breakdown curves were obtained in Fig. 2 to plot for the percentage of selected ions versus the varying collision energy. As can be seen, except the precursor ion, each fragment ion of the three isomers has drastically different content in a wide range of collision energies, which can be explained as the influence of the different substitution pattern. Decomposition of **[*o*-M$_1$+H]$^+$** almost only produces the fragment ion *m/z* 193, and the product ion (*m/z* 136) is unfeasibly generated at various activation energies. The product ion *m/z* 136 of **[*m*-M$_1$+H]$^+$** has significantly higher percentage of the total ion abundance than that of **[*p*-M$_1$+H]$^+$** within different collision energies, although both are abundant in the MS/MS.

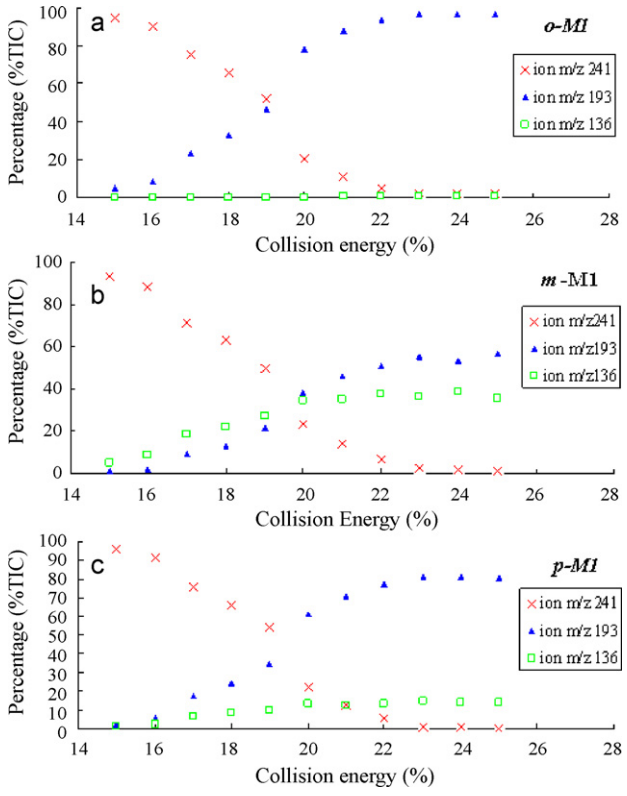

Fig. 2. Breakdown curves of selected ions (ions at *m/z* 241, *m/z* 193 and *m/z* 136) for **[*o*-M$_1$+H]$^+$** (a), **[*m*-M$_1$+H]$^+$** (b) and **[*p*-M$_1$+H]$^+$** (c).

Eliminations of CH_3SH and (NSC)SCH_3 are also the two main fragmentation channels for the chloro substituted isomers **M$_2$** (Fig. 1S, and Table 1). Different to the methoxyl-substituted isomers, however, the three chloro substituted isomers share the similar MS/MS, and they can not be easily differentiated by tandem MS of the protonated isomers.

In summary, the *ortho*, *meta* or *para* positional isomers of S-methyl methoxyl-benzenylmethylenehydrazine dithiocarboxylate have been differentiated according their different tandem MS behaviors due to the effect of the positional pattern. Decomposition of the *ortho*-isomer almost generates the fragment ion *m/z* 193 via CH_3SH elimination, and the other product ion *m/z* 136 via elimination of (NSC)SCH_3 is hardly produced. The fragment ion *m/z* 136 of *meta*-isomers is significantly more abundant than that of the *para*-one, although both are abundant. The chloro substituted isomers, however, share the similar MS/MS, and can hardly be distinguished by ESI-MS^2 techniques.

4. Mechanisms of positional factors and theoretical calculations

The different abundance of fragment ions in the CID-MS, applicable for recognizing the positional isomers, is viewed as a result of the different reactivity of the dissociation. The dissociation chemistry of their analogs, S-methyl benzenylmethylenehydrazine dithiocarboxylate, has been investigated in detail in our previous work [37]. Herein, DFT calculations at the B3LYP/6-31+G(2d,p) level were carried out to further investigate the mechanism of the positional effect on the two main dissociation reactions of the precursor ions in detail.

4.1. Structures of the protonated molecules

Both the imine N2 and the thiocarbon S5 in the structure can potentially prefer to accommodate the "ionzing" proton to form two isomers, **MH-a** and **MH-c**, respectively, and they can effectively interconvert each other through 1,5-proton migration [37]. The S5-protonated isomer **MH-c** is thermodynamically more stable than **MH-a** for the non-substituted compound. The imine N2, however, is more favorable for protonation in the *o*- and *p*-methoxyl-substituted compounds (Table 2), due to the "*ortho* effect" and the resonance stability of the substituent.

Fig. 3 displays the optimized structures of the N2-protonated methoxyl-substituted isomers (**M$_1$H-a1**). Due to the different orientation of the substituent position, both the *meta*- and the *ortho*-isomers have two conformational structures, respectively. The two conformational structures of the *meta*-isomer, ***m*1-MH-a1** and ***m*2-MH-a1**, share similar geometry parameters and nearly equivalent potential energy; whereas the two conformational

Table 2
Free energy (hartree) and relative free energy (kJ/mol) of the key species of CH_3SH elimination for the protonated title isomers.

	Structure	**o1**		**o2**		**m1**		**m2**		**p**	
		G (hartree)	Rel *G* (kJ/mol)	*G* (hartree)	Rel *G* (kJ/mol)	*G* (hartree)	Rel *G* (kJ/mol)	*G* (hartree)	Rel *G* (kJ/mol)	*G* (hartree)	Rel *G* (kJ/mol)
R = MeO–	**M_1H-c1**	−1369.60579	6.4	−1369.6024	15.3	−1369.60281	14.2	−1369.60277	14.3	−1369.608226	0.0
	M_1H-a1	−1369.606319	5.0	−1369.612059	−10.1	−1369.601633	17.3	−1369.601891	16.6	−1369.609353	−3.0
	M_1H-a1-TS1	−1369.553436	143.9	−1369.558766	129.9	−1369.549482	154.2	−1369.549638	153.8	−1369.556921	134.7
	$P_1$1 (*m*/*z* 193)	−438.689083	–	−438.689083	–	−438.689083	–	−438.689083	–	−438.689083	–
	CH_3SH	−930.905945	–	−930.912648	–	−930.900598	–	−930.900985	–	−930.909836	–
	$P_1$1 + CH_3SH	−1369.595028	34.7	−1369.601731	20.0	−1369.589681	51.6	−1369.590068	50.6	−1369.598919	27.4
	Ea		138.9		140.0		140.0		139.5		137.7
	Δ*G*		29.7		27.2		34.5		33.4		27.4
R = Cl–	**M_2H-c1**	−1714.698975	4.8	−1714.696104	12.3	−1714.699000	4.7	−1714.69922	4.1	−1714.700792	0.0
	M_2H-a1	−1714.69564	13.5	−1714.697283	9.2	−1714.69527	14.5	−1714.695489	13.9	−1714.698217	6.8
	M_2H-a1-TS1	−1714.6433	151.0	−1714.644671	147.3	−1714.643453	150.5	−1714.643749	149.8	−1714.646125	143.5
	$P_2$1 (*m*/*z* 197)	−1275.993574	–	−1275.997338	–	−1275.993304	–	−1275.993737	–	−1275.996953	–
	$P_2$1 + CH_3SH	−1714.682657	47.6	−1714.686421	37.7	−1714.682387	48.3	−1714.68282	47.2	−1714.686036	38.7
	Ea		146.2		138.1		145.8		145.7		143.5
	Δ*G*		42.8		25.4		43.6		43.1		38.7

structures of the *ortho*-isomer display distinct differences due to the *ortho*-effect.

An intramolecular hydrogen bond, 1.967 Å of the N2–H···O type, with a six membered ring exists in one of conformational structure (***o2*-M_1H-a1**) of the *ortho*-isomer (Fig. 3), according to calculated results. The intramolecular hydrogen bond in ***o2*-M_1H-a1** promotes the p–π conjugation between N3 and N2, witnessed by the N2–N3 bond length, which is much shorter than that in the other conformational structure **o1-M_1H-a1** (1.362 Å versus 1.376 Å). The N2–N3 bond in **o2-M_1H-a1** then shares more characters of double bond than that in other structures, with H7 nearly coplanar to the C1–N2–N3 plane (ΦC1–N2–N3–H7, −5.6°). Provided by the extra stability of the intramolecular hydrogen bond, ***o2*-M_1H-a1** is actually at the global minimum on our calculated energy surfaces of the protonated methoxyl-substituted isomers, and 25.4 kJ/mol lower in free energy than the S5-protonated isomer ***o2*-M_1H-c1** (Table 2), indicating that the *ortho* isomer exists almost as structure ***o2*-M_1H-a1**. The intramolecular hydrogen bond also significantly affects the fragmentation behavior of the precursor ion (see later section).

Besides the intramolecular hydrogen bond, the resonance effect of the methoxyl group also influences the geometry parameters of the protonated molecules. As shown in Fig. 3, the O–C_{Ph} and the C1–C_{Ph} bond lengths in the ***p*-M_1H-a1** are 0.016 and 0.017 Å shorter than those in the *meta* isomer, respectively, indicating that the substituent at the *para* site shares more conjugation with the C1=N2 double bond than that at the *meta* one. As an electron endowing group, the methoxyl group at the *para*- (or *ortho*-) site provides the extra stability of the N2-protonated isomers, by dispersing the positive charge on N2 upon protonation. As a result, the *para* isomer ***p*-M_1H-a1** is about 14 kJ/mol lower in energy than the *meta* one, and

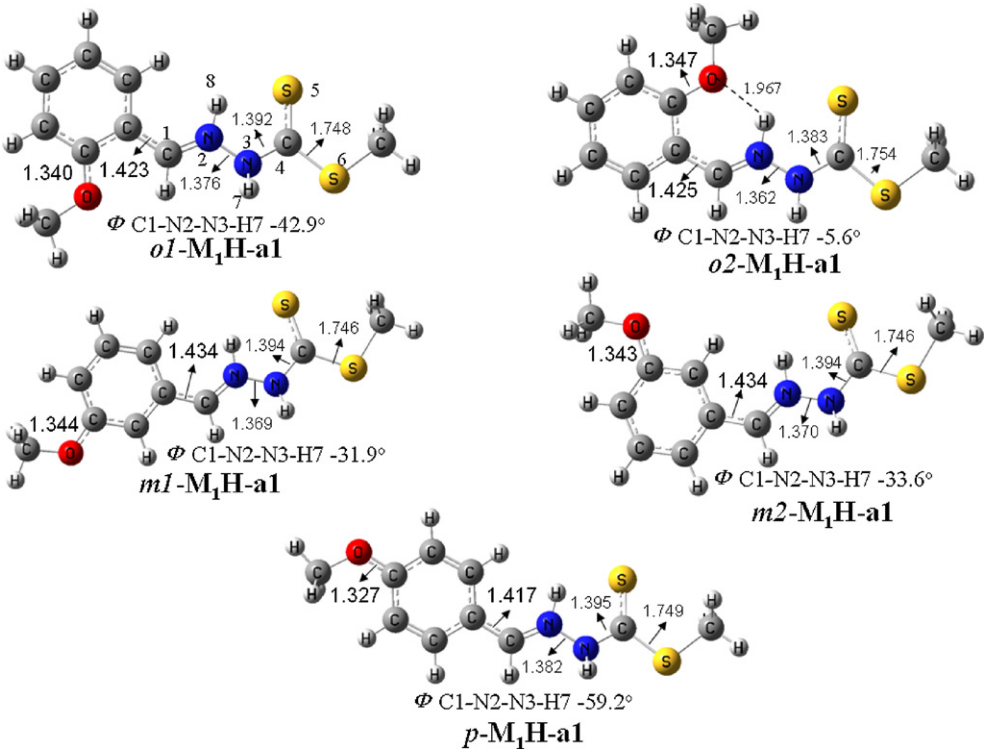

Fig. 3. Optimized structures **M_1H-a1** of the N2-protonated methoxyl-substituted isomers for the title compounds at B3LYP/6-31+(2d,p).

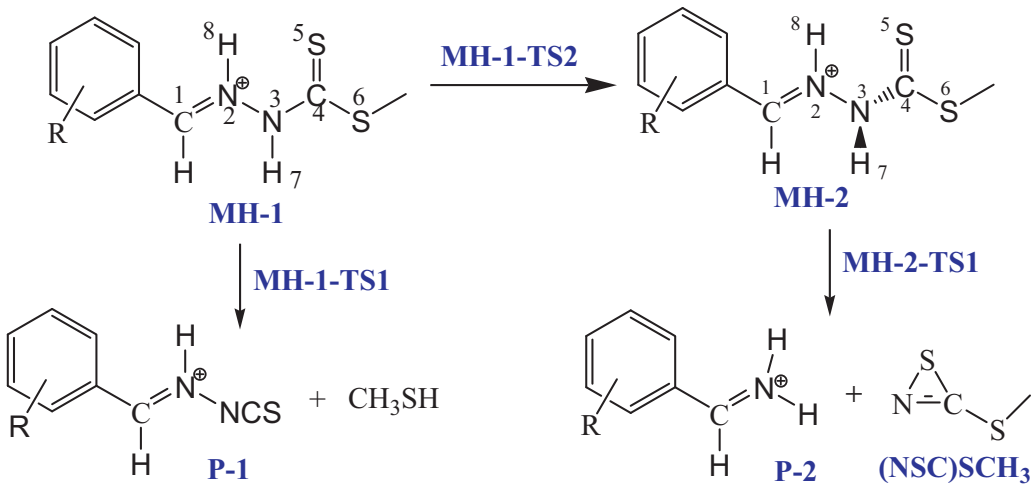

Scheme 2. The mechanism of the two main fragmentation reactions observed in CID-MS of the protonated isomers.

is also thermodynamically more favorable than the S5-protonated ones ***p*-M$_1$H-c** (Table 2).

4.2. Fragmentation of losing CH_3SH

CH_3SH dissociation of the protonated molecules is the most predominant fragmentation channel for the title compounds. Similar to decomposition of its neutral analogs [36], CH_3SH elimination is described as one-step reaction (Scheme 2), migration of the thiocarbamide hydrogen H7 to the methyl mercapto group S6 concomitantly with the breakage of the S6–C4 bond via a four-membered ring transition state **MH-a1-TS1** (Fig. 2S) [37]. Analysis of Table 2 shows that similar energy barrier of ~139 kJ/mol is shared for all the protonated methoxyl-substituted isomers, and about ~145 kJ/mol for the protonated chloro-substituted isomers. The calculated results indicate that the reactivity is almost immune to the substitution pattern on the phenyl ring, since the reaction center is away from the phenyl group.

However, different substituent affects the stability and then the relative abundance of the precursor ions, due to its different electronic effect. As shown in Table 2, the calculated energy barrier in the CH_3SH dissociation of the methoxyl-substituted compounds is about 6 kJ/mol lower in free energy than that of the chloro-substituted ones, indicating a more accessible reaction channel. As a result, less abundant precursor ions were observed in the tandem mass spectra of the methoxyl-substituted isomers than that of the chloro ones.

4.3. Fragmentation of losing $(NSC)SCH_3$

$(NSC)SCH_3$ (105 Da) elimination of the precursor ion **MH-a1**, which results in structurally diagnostic ions, is viewed as a two-step pathway (Scheme 2) [37]. In the first step, rotation of the thioamide group around the N2–N3 bond generates a conformational isomer **MH-a2**, with a low energy barrier (~40 kJ/mol) via **MH-a1-TS2** (Table 3). This process weakens the N2–N3 bond by breaking the p–π conjugation between N3 and N2, witnessed by extension of the N2–N3 bond length, e.g., to 1.394 Å in ***p*-M$_1$H-a2** from 1.382 Å in ***p*-M$_1$H-a1** (Fig. 3 and Fig. 3S). The subsequent breakage of the N2–N3 bond is induced by the adjacent positive charge on N2, concomitantly with transferring thioamide hydrogen to the N2 atom, and leads to product ion *m/z* 136 via **MH-a2-TS1** (Fig. 3S). Analysis of Table 3 indicates that the second step via **MH-a2-TS1** is the key step in this fragmentation.

Table 3
Free energy (hartree) and relative free energy (kJ/mol) of the key species of $(NSC)SCH_3$ elimination for the protonated title isomers.

	Structure	o1		o2		m1		m2		p	
		G (hartree)	Rel *G* (kJ/mol)	*G* (hartree)	Rel *G* (kJ/mol)	*G* (hartree)	Rel *G* (kJ/mol)	*G* (hartree)	Rel *G* (kJ/mol)	*G* (hartree)	Rel *G* (kJ/mol)
R = MeO–	**M$_1$H-c1**	−1369.60579	6.4	−1369.6024	15.3	−1369.60281	14.2	−1369.60277	14.3	−1369.608226	0.0
	M$_1$H-a1	−1369.606319	5.0	−1369.612059	−10.1	−1369.601633	17.3	−1369.601891	16.6	−1369.609353	−3.0
	M$_1$H-a1-TS2	−1369.59308	39.8	−1369.598931	24.4	−1369.588869	50.8	−1369.587135	55.4	−1369.5948	35.2
	M$_1$H-a2	−1369.598889	24.5	−1369.603922	11.3	−1369.593073	39.8	−1369.593447	38.8	−1369.602888	14.0
	M$_1$H-a2-TS1	−1369.538363	183.4	−1369.541129	176.2	−1369.537753	185.0	−1369.537746	185.0	−1369.541327	175.6
	P$_1$2 (*m/z* 136)	−440.510995	–	−440.515933	–	−440.504478	–	−440.504965	–	−440.515385	–
	(NSC)SCH$_3$	−929.071684	–	−929.071684	–	−929.071684	–	−929.071684	–	−929.071684	–
	P$_1$2 + (NSC)SCH$_3$	−1369.582679	67.1	−1369.587617	54.1	−1369.576162	84.2	−1369.576649	82.9	−1369.587069	55.5
	Ea1		34.7		34.5		33.5		39.8		38.2
	Ea2		178.4		186.3		170.8		170.7		178.6
	ΔG		60.7		64.1		70.0		68.6		58.5
R = Cl–	**M$_2$H-c1**	−1714.698975	4.8	−1714.696104	12.3	−1714.699000	4.7	−1714.69922	4.1	−1714.700792	0.0
	M$_2$H-a1	−1714.695600	13.5	−1714.697283	9.2	−1714.69527	14.5	−1714.695489	13.9	−1714.698217	6.8
	M$_2$H-a2-TS1	−1714.632673	178.8	−1714.634104	175.1	−1714.634326	174.5	−1714.634635	173.7	−1714.635759	170.7
	P$_2$2 (*m/z* 140)	−785.597014	–	−785.59935	–	−785.596576	–	−785.596997	–	−785.600891	–
	P$_2$2 + (NSC)SCH$_3$	−1714.668698	84.3	−1714.671034	78.1	−1714.66826	85.4	−1714.668681	84.3	−1714.672575	74.1
	Ea2		174.0		165.9		169.8		169.6		170.7
	ΔG		79.5		68.9		80.7		80.2		74.1

Table 4
The Breneman charge distribution of some key atoms in the optimized N2-protonated isomers **M_1H-a2**.

Structure	N2	O	H8	N3
***o1*-M_1H-a2**	0.1372	−0.3271	0.2137	−0.3776
***o2*-M_1H-a2**	0.1289	−0.3860	0.2373	−0.3756
***m1*-M_1H-a2**	0.2017	−0.3463	0.1944	−0.3955
***m2*-M_1H-a2**	0.2156	−0.3500	0.1989	−0.3839
***p*-M_1H-a2**	0.1845	−0.3340	0.1965	−0.3742

Since the methoxyl substituent at the *para* site shares more resonance with the C1=N2 double bond, the N2 atom in structure ***p*-M_1H-a2** contains less positive charge than that in ***m*-M_1H-a2**, due to the strong electron donating effect of the methoxyl group. As shown in Table 4, the calculated Breneman charge on the N2 atom is 0.1845 in ***p*-M_1H-a2**, which is less than that in the *meta* one (0.2017 for ***m1*-M_1H-a2** or 0.2156 for ***m2*-M_1H-a2**). Less positive charge on N2 atom means less polarization of the neighboring N2–N3 bond. Therefore, (NSC)SCH_3 elimination of ***p*-M_1H-a2** has about 8 kJ/mol higher calculated energy barrier than that of ***m*-M_1H-a2** (Table 3). The above calculations results are in good consistent with CID-MS results, in which the corresponding fragment ion (*m/z* 136) of ***p*-M_1H** is significantly less abundant than that of ***m*-M_1H** (Table 1).

Due to the *ortho* effect (hydrogen bond) and the electron donating resonance, the calculated Breneman charge on N2 is only 0.1289 in the *ortho*-methoxyl-substituted isomer ***o2*-M_1H-a2**, which is far less than that in the other isomers (Table 4). The energy barrier for (NSC)SCH_3 elimination of ***o2*-M_1H-a2** then significantly increases to 186.3 kJ/mol, which is about 8 kJ/mol higher in free energy than that for the *para* isomer, and about 18 kJ/mol higher than that for the *meta* one. As a result, (NSC)SCH_3 elimination of the *ortho*-isomer is further suppressed, and the relevant product ion *m/z* 136 is extremely low in abundance (0.4%) in the tandem MS of ***o*-M_1H**, which is abundant in the MS/MS of the *para* or the *meta* isomer.

The chloro substituent, however, is a group with weak electronic effect, and thereby both the *meta*- and *para*-isomers (***p*-M_2H** and ***m*-M_2H**) have similar energy barriers in the process of (NSC)SCH_3 elimination (Table 3). The chloro substituent at the *ortho* site does not interact strongly with the ionizing proton on the imine N2 atom with hydrogen bond, and then hardly alerts the energy barrier in the process of fragmentation. As results, the corresponding product ions display similar abundance in the tandem mass spectra (Table 1 and Fig. 1S).

5. Conclusion

In this paper, the *ortho*, *meta* or *para* positional isomers of S-methyl methoxyl- (or chloro-) substituted benzenylmethylene-hydrazine dithiocarboxylate, RPhCH=N–NHC(=S)–SCH_3 (R = MeO– or Cl–), have been investigated by collision induced dissociation mass spectrometry. Eliminations of CH_3SH and (NSC)SCH_3 are the two main fragmentation channels of the protonated molecules. The fragment ion *m/z* 136 resulting from (NSC)SCH_3 elimination displays significant difference in the relative abundance for the three methoxyl-substituted isomers, indicating that these positional isomers were differentiated solely by tandem MS. The chloro-substituted isomers, however, show no distinct difference in the CID-MS.

The different abundance of the characteristic ions in the CID-MS is as a result of the varying dissociation reactivity, due to the positional effect. The calculation results revealed that the energy barrier of CH_3SH elimination is almost immune to the substitution pattern on the phenyl ring for both methoxyl- and chloro-substituted isomers, since the reaction center is away from the phenyl group.

Elimination of (NSC)SCH_3 is triggered by the positive charge upon protonation on the imine N2. The positive charge on N2 in the *para* isomer is dispersed due to the p–π conjugation effect of the methoxyl group, and thereby the relevant energy barrier in dissociation of the *para* isomer is ~8 kJ/mol higher in free energy than that of the *meta* one. As a result, the corresponding product ion (*m/z* 136) of the *para* isomer is distinctly less abundant than that of the *meta* one (22.0% and 57.7%). The methoxyl substituent at the *ortho* position further suppresses the (NSC)SCH_3 elimination channel, due to both the resonance effect and the intramolecular hydrogen bond in the N2-protonated isomer ***o2*-M_1H-a2**, with much higher energy barrier and then extremely low abundant the product ion (*m/z* 136, 0.4%). In comparison, all the three chloro-substituted isomers are short of the above positional effects due to the weak electronic effect of the substituent, have the similar calculated energy barrier in (NSC)SCH_3 elimination, and then share the similar tandem MS.

Acknowledgments

The National Science Foundation of China for Grant NSFC-20975092 supports this work. Computer time was made available on the SGI Aktix 450 sever at Computational Center for Molecular Design of Organosilicon Compounds, Hangzhou Normal University.

Appendix A. Supplementary data

Supplementary data associated with this article can be found, in the online version, at doi:10.1016/j.ijms.2010.09.004.

References

[1] K.M. Barkigia, M.D. Berber, J.C. Fajer, J. Medforth, M.W. Renner, K.M. Smith, J. Am. Chem. Soc. 112 (1990) 8851–8857.
[2] H.K. Hombrecher, V.M. Gherdan, S. Ohm, J.A.S. Cavaleiro, M.G.P.M.S. Neves, M.F. Condesso, Tetrahedron 49 (1993) 8569–8577.
[3] T.J. Dingemans, E. Mendes, J.J. Hinkley, E.S. Weiser, T.L. StClair, Macromolecules 41 (7) (2008) 2474–2483.
[4] M.A.P. Segurado, J.C.R. Reis, J.D.G. Oliveira, S. Kabilan, M. Shanthi, J. Org. Chem. 72 (14) (2007) 5327–5336.
[5] F. Effenberger, A.H. Maier, J. Am. Chem. Soc. 123 (15) (2001) 3429–3433.
[6] F.E.M.E. Hegazy, S.Z.A. Fattah, E.A. Hamed, S.M. Sharaf, J. Phys. Org. Chem. 13 (9) (2000) 549–554.
[7] J. Das, C.V.L. Rao, T.V.R.S. Sastry, M. Roshaiah, P.G. Sankar, A. Khadeer, M.S. Kumar, A. Mallik, N. Selvakumar, J. Iqbal, S. Trehan, Bioorg. Med. Chem. Lett. 15 (2) (2005) 337–343.
[8] C.L. Rojas, F.J. Romera, E. Alcantara, R. Perez-Vicente, C. Sariego, J.I. Garcia-Alonso, J. Boned, G. Marti, J. Agric. Food Chem. 56 (2008) 10774–10778.
[9] B. Milos, P. Zdenko, S. Jirina, Oxytocin and its analogs, Protein Pept. Lett. 12 (2005) 343–347.
[10] B.R. Stanmore, Combust. Flame 136 (398) (2004) 427.
[11] M. Begala, G. Tocco, G. Meli, G. Podda, S.A.M. Urru, J. Mass Spectrom. 44 (2009) 245–251.
[12] M.R.M. Domingues, -Marques S.F M.G.O., P. Domingues, M.G. Neves, J.A.S. Cavaleiro, A.J. Ferrer-Correia, O.V. Nemirovskiy, M.L. Gross, J. Am. Soc. Mass Spectrom. 12 (2001) 381–384.
[13] M.A. Mends, R. Rittner, M.N. Eberlin, Eur. J. Mass Spectrom. 8 (2002) 27–33.
[14] D. Błachut, W. Danikiewicz, M. Olejnik, Z. Czarnocki1, J. Mass Spectrom. 39 (2004) 966–972.
[15] F.B. Jariwala, M. Figus, A.B. Attygalle, J. Am. Soc. Mass Spectrom. 19 (2008) 1114–1118.
[16] Z. Chen, J.-M. Lin, K. Uchiyama, T. Hobo, J. Chromatogr. A 813 (2) (1998) 369–378.
[17] J.A. Sellers, B.A. Olsen, P.K. Owens, P.F. Gavin, J. Pharm. Biomed. Anal. 41 (4) (2006) 1088–1094.
[18] A. Jakab, I. Jablonkai, E. Forgács, Rapid Commun. Mass Spectrom. 17 (20) (2003) 2295–2302.
[19] D. Swain, R.E. Winans, W.J. Dunn, Anal. Chem. 68 (18) (1996) 3244–3249.
[20] V.P. Joshi, M.G. Kulkarni, R.A. Mashelkar, J. Chromatogr. A 849 (2) (1999) 319–330.
[21] V.G. Dongre, P.P. Karmuse, M.M. Nimbalkar, D. Singh, J. Kuma, Pharm. Biomed. Anal. 39 (1–2) (2005) 111–116.
[22] T. Chasse, R. Wenslow, Y. Bereznitski, J. Chromatogr. A 1156 (1–2) (2007) 25–34.
[23] W.A. Tao, F.C. Gozzo, R.G. Cooks, Anal. Chem. 73 (2001) 1692.
[24] J.-Y. Salpin, J. Tortajada, J. Mass Spectrom. 37 (2002) 379.
[25] E.C. Kempen, J. Brodbelt, J. Mass Spectrom. 32 (1997) 846.
[26] F. Kjeldsen, K.F. Haselmann, E.S. Sorensen, R.A. Zubarev, Anal. Chem. 75 (2003) 1267.
[27] F.F. Hsu, J. Turk, M.L. Gross, J. Mass Spectrom. 38 (2003) 447.
[28] Y.E. Corilo, M.N. Eberlin, J. Mass Spectrom. 43 (2008) 1636–1640.

[29] M. Carvalho, F.C. Gozzo, M.A. Mendes, R. Sparrapan, C. Kascheres, M.N. Eberlin, Chem.-Eur. J. 4 (1998) 1161.
[30] L.A.B. Moraes, A.A. Sabino, E.C. Meurer, M.N. Eberlin, J. Am. Soc. Mass Spectrom. 16 (2005) 431–436.
[31] G. Hopfgartner, E. Bourgogne, Quantitative high-throughput analysis of drugs in biological matrices by mass spectrometry, Mass Spectrom. Rev. 22 (2003) 195.
[32] A.S. Fang, X. Miao, P.W. Tidswell, M.H. Towle, W.K. Goetzinger, J.N. Kyranos, Mass Spectrom. Rev. 27 (2008) 20.
[33] J. Wang, Mass Spectrom. Rev. 28 (2009) 50.
[34] D.L. Klayman, J.F. Bartosevich, T.S. Griffin, C.J. Mason, J.P. Scovill, J. Med. Chem. 22 (1979) 7855–7862.
[35] R. Lin, P.J. Connolly, S. Huang, S.K. Wetter, Y. Lu, W.V. Murray, S.L. Emanuel, R.H. Gruninger, A.R. Fuentes- Pesquera, C.A. Rugg, S.A. Middleton, L.K. Jolliffe, J. Med. Chem. 48 (13) (2005) 4208–4211.
[36] K.-Z. Jiang, G.-F. Bian, H.-Y. Qiu, Y.-J. Pan, G.-Q. Lai, J. Phys. Chem. A. 113 (4) (2009) 697–706.
[37] K.-Z. Jiang, G.-F. Bian, N. Hu, Y.-J. Pan, G.-Q. Lai, Int. J. Mass Spectrom. 291 (2010) 17–23.
[38] L.Z. Chen, G.F. Bian, K.Z. Jiang, J.R. Wu, G.Q. Lai, Acta Chim. Sinica 65 (17) (2007) 1897–1901.
[39] The relative collisional energy in this ion trap instrument (LCQ) varies from 0 to 100%, where 0–100% relative collisional energy correspond to 0–5 V peak to peak of the resonance excitation RF voltage, e.g. 20% relative collisional energy means 1 V (5 V × 20%).
[40] M.J. Frisch, G.W. Trucks, H.B. Schlegel, G.E. Scuseria, M.A. Robb, J.R. Cheeseman, V.G. Zakrzewski, J.A. Montgomery Jr., R.E. Stratmann, J.C. Burant, S. Dapprich, J.M. Millam, A.D. Daniels, K.N. Kudin, M.C. Strain, O. Farkas, J. Tomasi, V. Barone, M. Cossi, R. Cammi, B. Mennucci, C. Pomelli, C. Adamo, S. Clifford, J. Ochterski, G.A. Petersson, P.Y. Ayala, Q. Cui, K. Morokuma, D.K. Malick, A.D. Rabuck, K. Raghavachari, J.B. Foresman, J. Cioslowski, J.V. Ortiz, B.B. Stefanov, G. Liu, A. Liashenko, P. Piskorz, I. Komaromi, R. Gomperts, R.L. Martin, D.J. Fox, T. Keith, M.A. Al-Laham, C.Y. Peng, A. Nanayakkara, C. Gonzalez, M. Challacombe, P.M.W. Gill, B. Johnson, W. Chen, M.W. Wong, J.L. Andres, C. Gonzalez, M.E. Head-Gordon, S. Replogle, J.A. Pople, Gaussian 03 Inc., Pittsburgh PA, 2003.